J Mater Sci (2015) 50:4860–4878
DOI 10.1007/s10853-015-9029-6

Spark plasma sintering of commercial and development titanium alloy powders

N. S. Weston[1] · F. Derguti[1] · A. Tudball[2] · M. Jackson[1]

Received: 4 February 2015 / Accepted: 15 April 2015 / Published online: 29 April 2015

Abstract Emerging lower cost titanium metal powder produced via an electrolytic method has been fully consolidated using spark plasma sintering (SPS) generating microstructures comparable to those observed in Ti–6Al–4V PM product. This is the first time powder from an alternative titanium extraction method has been processed via SPS and it is benchmarked with commercial alloys (CP–Ti, Ti–6Al–4V, and Ti–5Al–5V–5Mo–3Cr). The effect of powder feedstock size, morphology, and alloy chemistry on the consolidated density and microstructure is presented. Through a design of experiments (DoE) type approach the effect of SPS processing conditions on these alloy powders, including maximum sintering temperature, pressure, heating rate, and dwell time were investigated. The SPS process is found to be largely insensitive to feedstock size and morphology, although very large or highly porous powder particles are more difficult to fully consolidate. The maximum sintering temperature and pressure have the largest contribution to achieving full consolidation, with higher pressures and temperatures increasing the final density. Increasing heating rate increases the final grain size, despite less time being spent at the higher temperature and it is thought this is due to bypassing the traditional first phase of sintering. This paper shows that SPS is a viable step for a low-cost manufacturing route, for example to produce preform billets to be finished with a one-step forging operation, especially when combined with the possibility of lower cost powder. In the long-term, SPS will allow a significant reduction in the processing cost, contributing to an increased usage of titanium powder feedstock for a range of applications. This is reinforced by the successful large scale production of a 5 kg SPS Ti-6-4 billet, demonstrating the potential industrial scalability of the process, particularly for the aerospace industry.

✉ N. S. Weston
nsweston1@sheffield.ac.uk

F. Derguti
f.derguti@sheffield.ac.uk

A. Tudball
adam.tudball@kennametal.com

M. Jackson
martin.jackson@sheffield.ac.uk

[1] Department of Materials Science and Engineering, The University of Sheffield, Sir Robert Hadfield Building, Mappin Street, Sheffield S1 3JD, UK

[2] Kennametal Manufacturing (UK) Ltd, Lake Road, Leeway Industrial Estate, Newport, South Wales NP19 4SR, UK

Introduction

Titanium alloys have a unique combination of properties with strength comparable to steels, but at approximately 60 % of the density, giving one of the best specific strengths of any structural metal. Combine this with a high melting point, low thermal expansion, excellent corrosion resistance, and biocompatibility, and titanium alloys become highly desirable materials. Titanium is the ninth most abundant element in the Earth's crust; although its high affinity for oxygen makes extraction from the ore and subsequent processing and fabrication challenging. This is currently reflected by the extreme cost of titanium products, which limits their use to situations where the superior combination of properties outweighs the price penalty; typically the aerospace and chemical plant industries, biomaterial applications, and marine environments. Lowering the cost of titanium to a level where it can become a

twenty-first century commodity metal is therefore of considerable interest.

A lower cost extraction method, and substitute to the 60-year-old Kroll process, is one small part of the solution to lowering the price of titanium. Several alternative titanium extraction methods, including electrolytic processes and continuous Kroll-type reactions, are currently being developed but none are yet operating commercially [1–3]. The Metalysis FFC process is one such method, which reduces titanium ore to metal through electrolysis in a molten salt bath [4, 5]. However, Fig. 1 demonstrates that lower cost extraction alone will not achieve the desired reduction in the overall price of titanium due to almost half the final cost arising from downstream ingot processing; this proportion will only increase as the complexity of a finished component grows. Significantly, a number of the developing lower cost extraction processes produce particulate or powder products. It is highly desirable to process these titanium alloy powders into fully consolidated semi-finished parts with properties equal to or greater than conventionally processed wrought material. Consolidation of these low-cost materials will almost certainly have to be via a non-melt route utilising powder metallurgy (PM) techniques, thus removing many of the costly and time consuming traditional processing steps. This will enable a step-change in economics that will allow titanium alloy usage in areas where price has historically been prohibitive [2, 6–9]. A successful PM processing route offers great advantages to designers; production of near net shape parts, the ability to scale up to high rates of production, and reduction of multi-stage forging, thus offering significant cost savings. Another important advantage of PM with regards to titanium, due to its high affinity with oxygen [10], is that the material remains in the solid state.

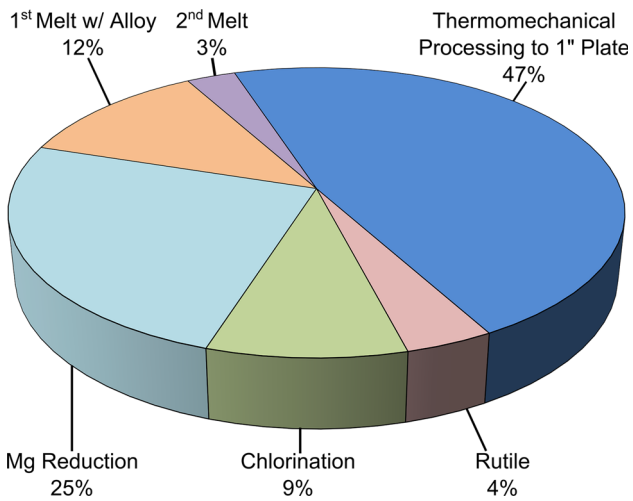

Fig. 1 Relative cost factors for conventional processing to produce 25 mm titanium alloy plate; produced from data reported by Kraft [1]

Most PM routes utilise sintering, which is the process of consolidating powders to make solid objects without melting the particles. The use of electric current to activate a rapid sintering process is a method that has been shown to consolidate titanium alloys; referred to variously as spark plasma sintering (SPS), field-assisted sintering technique (FAST), and pulsed electric current sintering (PECS). SPS combines the effects of axial mechanical loading with elevated temperature, via Joule heating from a direct and possibly pulsed electric current, to a mould assembly containing powder. The applied current allows very high heating rates to be achieved. SPS is reported to be a useful tool in the consolidation of numerous materials, many of which were traditionally considered difficult to consolidate; WC processed with a smaller grain size and improved properties in less than half the time by Eriksson et al. [11]. Whilst beyond the scope of this work, Orrù et al. have presented a thorough review of the wide variety of materials successfully processed via SPS [12].

Increasing process efficiency and saving energy is crucial in a low-cost processing route for titanium alloys and SPS clearly shows the potential to assist with this. The energy efficiency of SPS compared to conventional hot pressing is demonstrated by Musa et al. using Ti–Al_2O_3–TiC composites; the lower temperature and reduced time to produce a material with slightly improved properties via SPS led to a 90–95 % energy saving [13]. Whilst the precise saving will vary with conditions and materials, Musa et al. have demonstrated the significant cost reductions possible. Present commercial SPS systems most commonly use all graphite mould assemblies, which conduct with a higher resistivity than most metals, meaning it dissipates electrical energy to heat at reasonable current densities. Drawbacks of these assemblies include (1) current flows through the entire mould dissipating electrical energy over a large volume compared to the sample volume (2) current leaks through the die reducing sample current density and its positive effects (3) graphite conducts heat well resulting in high heat loss to surroundings requiring higher power input. However Chennoufi et al. used a mould assembly with a thermal/electrical insulation layer between stainless steel plungers and the ring, and heat-generating graphite foils between sample and plungers [14]. This insulation prevents leakage currents so that current density through the sample is maximised (up to three times higher than conventional all-graphite assemblies) also reducing heat loss to surroundings.

Whilst titanium alloys are suitable for processing by SPS there is relatively little published work. The economics of a low-cost processing route are less beneficial unless a low-cost feedstock is available and therefore titanium alloy PM routes have historically received less attention than more exotic materials. Published work falls

mainly into two categories: (1) the production of titanium alloys for biomedical applications and (2) production of ultrafine-grained (UFG) titanium alloys usually with a high energy ball milling stage preceding the sintering to produce the nano-crystalline microstructure to be preserved within the SPS machine. Handtrack et al. aimed to improve the biocompatibility of commercially pure titanium (CP–Ti) through increasing strength and wear resistance by producing UFG titanium containing Ti_5Si_3 dispersoids [15]. High energy ball milling was used to create nano-crystalline Ti–Si particles which were processed via SPS at a variety of temperatures and pressures. Strength comparable to, and hardness exceeding, Ti–6Al–4V were reported. Masaki et al. similarly claimed to be able to produce Ti_5Si_3 dispersoids within a titanium matrix, but starting with SiO_2 powder [16]. Nicula et al. and Sakamoto et al. both used the SPS process to produce titanium compacts with tailored porosity to improve biocompatibility [17, 18]. The porosity aimed to allow increased cell adhesion and osteo-integration as well as more closely matching the Young's modulus and strength of human bone. Both research teams reported successes with more closely matching bone properties and increased cell growth on porous substrates. SPS as a titanium joining technique has been investigated; He et al. showed it possible to join Ti–6Al–4V achieving a joint strength 91 % of the bulk alloy, greatly exceeding hot pressing results, and showed that grains and phases grew across the interface [19]. Miriyev et al. demonstrated a 250 MPa joint strength between Ti–6Al–4V and low-alloy AISI 4330 steel by SPS, with the advantage that the highly brittle intermetallic products found in conventional welding did not form due to a layer of TiC forming [20]. Other researchers have also demonstrated that fully dense titanium can be produced via SPS: Chaudhari et al., Menapce et al., and Eriksson et al. suggest that particle deformation is the most significant contribution to densification, rather than spark discharge or heating anisotropy at neck regions, due to the temperature of maximum densification rate during SPS coinciding with the maximum strain rate during compression testing [21–23]. They additionally state that increasing pressure led to more rapid compaction as well as current pulsing having little effect. Zadra et al. processed CP–Ti and showed that the material was almost fully dense at 800 °C, with small increases in density at higher temperatures and a rapid grain growth above the α–β transition temperature [24]. They also showed that interstitial content of carbon, oxygen, and nitrogen remains constant from the starting material independent of processing temperature and optimum mechanical properties achieved at 900 °C.

The SPS process appears to offer clear advantages with regards to powder consolidation, but there may also be disadvantages. Temperature and stress gradients across samples may lead to microstructural/compositional heterogeneity, especially in larger samples or near net shaped parts. Work by Muñoz et al. simulating the SPS process has shown that the temperature distribution inside samples is mainly controlled by their thermal conductivity; low conductivity leads to significant temperature gradients and high conductivity leads to homogeneous temperature distributions [25]. Anselmi-Tamburini et al. support this and additionally claim current density is also a large factor in temperature profiles; a higher local current density giving higher local heating [26]. They also reported simulations of copper where uniform stress was seen across most of the sample, both radially and axially. There is an exception at the edge where top and bottom saw significantly different stresses; this would possibly lead to differences in microstructure/density. They surmise that stress gradients play a more important role in sample microstructure during SPS due to their larger size.

The review papers by Munir et al. further show the overriding view that SPS provides benefits over traditional methods of sintering [27, 28]. These include the intrinsic advantages of lower sintering temperature and shorter processing times, as well as the reported improvement in comparative properties. These benefits are well reported within the literature but scientific explanation of them frequently falls short; the existence of "spark plasma" is regularly suggested as the reason for the improved processing through cleaning of particle surface layers, but little convincing evidence exists to support this [27]. It should also be noted that the reporting of lower temperature reduced time benefits combined with improved properties cannot necessarily be treated as independent factors; it is likely that in some cases the improved properties come from the lower temperature and shorter processing time leading to different compositions and microstructures. Not all property enhancements can be assigned to the lower temperature. The application of pressure and current in the SPS process can be shown to have beneficial effects when compared to methods such as pressureless sintering and hot pressing.

In summary, relatively little attention has been given to the processing of titanium alloy powder via an SPS route. Most studies are concerned with using the unique capabilities of SPS to retain UFG structures or retain porosity and not attain full density. Producing UFG titanium alloys entails starting with very small powder sizes and usually involves heavy pre-processing via high energy ball milling. This is not applicable in the case of a low-cost processing route due to the added cost, complexity, and particle size differing greatly from those produced via alternative extraction routes. The production of porous titanium also has little to offer when exceeding the properties of conventional wrought product is desired. The work presented here shows how feedstock size, morphology, and chemistry

affect the processing conditions required when consolidation is undertaken by SPS, including maximum sintering temperature and pressure, and hold time at these conditions, as well as heating rate. Titanium alloy powder from the Metalysis FFC process, a lower cost extraction route, was fully consolidated in one processing step, demonstrating that SPS is a viable tool in a low-cost processing route, perhaps as a precursor to one-step precision forging. The combination of a potentially low-cost feedstock with a low-cost processing method will, in the long-term, allow the significant reduction in cost required. There has been no published work on the SPS of titanium alloy feedstock produced via alternative extraction methods, and due to its scarcity much of this work will be undertaken with commercially available spherical gas atomised (GA) or angular hydride-dehydride (HDH) titanium alloy powders. These allow the concept of the consolidation method to be proven and also provide a comparison and benchmark. A small-scale laboratory consolidation route will be proved at the tens to hundreds of grams level, followed by a demonstration of true industrial scalability by the production of a 5 kg SPS disc. SPS machine data, sample density, microhardness, grain size and two-phase α–β morphology, and interstitial pick-up will be analysed to allow assessment of SPS as a low-cost processing step.

Materials and methods

Five alloys were selected for the work: Grade 2 CP–Ti, Ti–6Al–4V, Ti–5Al–5V–5Mo–3Cr, and two novel Metalysis alloy powders—one derived from natural rutile and the other from pigment grade titanium dioxide. The conventional alloys' morphology is either spherical or angular, whilst the Metalysis powder has a more porous nature in its raw form; although this can be removed with an additional spheroidisation processing step, see Table 1. Each powder feedstock was characterised to determine the effects of powder size, chemistry, and morphology on SPS processing. Light microscopy was used to assess morphology and microstructure. A Malvern Mastersizer 3000 gave a particle size distribution (PSD) for the powders; small amounts of each powder were wet dispersed through the machine and 20 measurements were taken to allow averaging. The system was thoroughly flushed and recalibrated between alloys to prevent cross-contamination. The GA CP–Ti and GA Ti-6-4 were purchased from Arcam. The HDH CP–Ti and HDH Ti-6-4 were purchased from Reading Alloys. All four materials were certified within ASTM specifications for the respective grade. The GA Ti-5553 was purchased from TLS Technik and was also within manufacturer's specifications. The chemistries for the Metalysis powder cannot be given as they are commercially sensitive at this stage of development; although they are achieving low levels of interstitial elements as can be seen in Table 3.

For the small-scale laboratory route, the powders were consolidated using an FCT Systeme GmbH Spark Plasma Sintering Furnace type HP D 25. The scaled up processing was performed with an FCT Systeme GmbH Spark Plasma Sintering Furnace type H-HP D 250 located at Kennametal Manufacturing (UK) Ltd.; the same methodology was used regardless of the size/mass of specimen or type of SPS furnace. The mass of powder, M, needed to achieve the desired specimen thickness when fully dense, t, can be calculated from Eq. 1, where ρ is the density of the selected alloy and r is the radius of the selected mould.

$$M = \rho t \pi r^2. \quad (1)$$

The powder was placed within a graphite ring mould, with two close-fitting cylindrical pistons located either side, and a carbon felt jacket added to help prevent radiative heat loss. This assembly was pre-lined with graphite foil before each processing run to aid with sample removal and prevent mould wear. The loaded mould was placed into the

Table 1 Titanium alloy powder feedstocks studied with information on their chemistry, morphology, and particle size distribution

Chemistry	Morphology	PSD Statistics			
		Dx (10) (μm)	Dx (50)(μm)	Dx (90) (μm)	Relative span
CP–Ti	Spherical	50.3	71.1	100	0.70
CP–Ti	Angular	38.6	77.2	135	1.25
Ti-6-4	Spherical	51.1	72.5	104	0.73
Ti-6-4	Angular	86.1	129	196	0.85
Ti-5553	Spherical	22.9	69	142	1.73
Rutile derived	Spherical	64.3	98.5	149	0.86
Rutile derived	Angular/spongy	94.7	150	231	0.91
Pigment derived	Angular/spongy	232	327	459	0.69
Pigment derived	Spherical/spongy	N/A	N/A	N/A	N/A

SPS furnace vacuum chamber, between two conducting rams hydraulically controlled to apply force during sintering, and a pre-programmed sintering cycle started. The following basic cycle was used for all experiments in this work, with hold temperature, hold pressure, heating rate, or dwell time changed appropriately, see Fig. 2. The chamber was evacuated, purged with argon, evacuated again, and re-purged with argon. Pulsed DC current was applied to the mould through the rams to start the heating process. Once the temperature reached 450 °C (point A on Fig. 2), a pyrometer viewing axially downwards onto the upper graphite piston's inner face was used to control the set heating rate up to the set hold temperature. The applied force stayed at 5 kN until the temperature reached 600 °C (point B on Fig. 2) when it began to increase at a rate so that the set hold pressure occurred simultaneously with the set hold temperature (point C on Fig. 2), followed by a set dwell period (points C–D). Finally, the current was turned off and the sample was allowed to cool until the vacuum chamber could be opened and the mould be removed. The sample was taken out of the mould and the graphite paper was removed by grit blasting. Samples of interest were then examined microscopically.

The design of experiments type approach was used to assess how GA CP–Ti, HDH CP–Ti, angular/spongy rutile-derived and spherical/spongy pigment-derived alloys behave in the machine, with density as the measured outcome. The two factors varied were hold temperature and hold pressure as the literature suggests these have the largest influence. A two factor central composite design study was used with 10 experimental points; consisting of an imbedded two level full factorial design (750 °C-25 MPa, 750 °C-45 MPa, 950 °C-25 MPa, 950 °C-45 MPa) augmented by star points to expand the design space (709 °C-35 MPa, 850 °C-21 MPa, 850 °C-49 MPa, 991 °C-35 MPa) and a centre point to check for response curvature (850 °C-35 MPa), plus an additional outlying point (1200 °C-35 MPa) to check material response at higher temperature. The software randomised the order of the experimental runs to help negate systematic errors; see Table 2 for further details. Once a hold temperature and pressure combination which consistently produced full density were found, the heating rate and dwell time were varied at these conditions to evaluate their effect on processing output for HDH CP–Ti, HDH Ti-6-4, GA Ti-5-5-5-3, and spheroidised rutile-derived alloy. Heating rates were changed between 25, 50, 100, and 200°C min^{-1}. Dwell time was increased from 10 to 20, to 30, and then to 60 min.

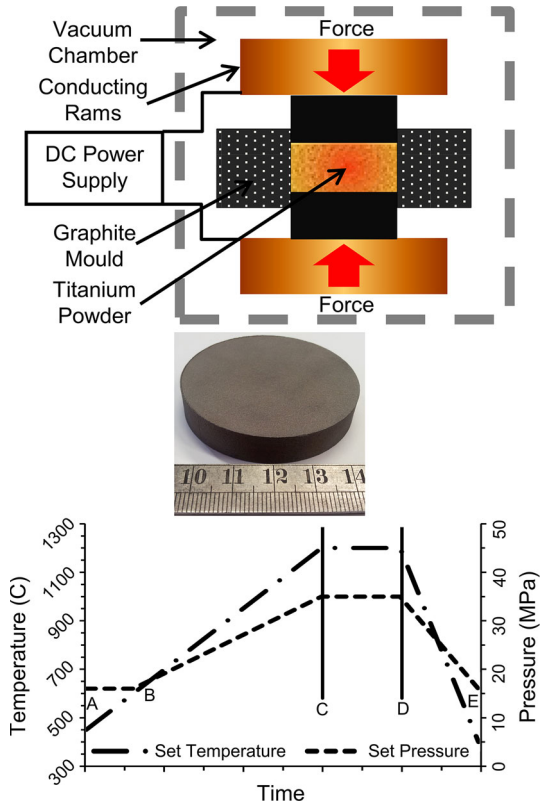

Fig. 2 *Top* Schematic diagram of SPS furnace layout. *Middle* Example of titanium disc produced via SPS. *Bottom* Schematic graph of SPS process cycle

Standard metallographic preparation for titanium alloys was used for all samples: hot-mounting in conductive Bakelite or cold-mounting in epoxy resin, followed by grinding and polishing using silicon carbide papers, then 9 μm diamond suspension, and finally a chemical/mechanical polish using colloidal silica of 0.05 μm mixed with 20 % hydrogen peroxide. Observation of microstructure and porosity was performed in a Nikon Eclipse LV150 light microscope under reflected light conditions, both in bright field and polarised light mode. If needed Kroll's reagent was applied as an etchant to the fully polished samples for 8–12 s to show increased microstructural detail.

The density of samples was checked using Archimedes method; the samples were coated in wax to prevent water intrusion into any remaining open porosity providing a more accurate value of density. This method was complemented by image analysis of bright field light micrographs, using the software ImageJ [29]. The micrographs were converted to 8-bit grayscale and then into black and white using a threshold algorithm; the porosity is calculated from the percentage of black pixels present. An average value for eleven images, captured across each sample, was measured to help alleviate any geometry effects or anomalies. The resulting two density values were finally averaged.

Microhardness testing was performed using a Struers Durascan-70. Metallographically prepared samples were indented using a Vickers hardness tip with a mass of 1 kg

Table 2 Calculated densities for GA and HDH CP–TI, as well as pigment and rutile-derived Metalysis alloys, at varying levels of hold temperature and hold pressure during SPS

Run	Temp. (°C)	Pressure (MPa)	GA CP–Ti density (%)	HDH CP–Ti density (%)	Spherical/spongy pigment-derived density (%)	Angular/spongy rutile-derived density (%)
1	991	35	99.8	99.9	97.8	97.8
2	750	45	97.5	97.1	92.9	92.7
3	750	25	90.5	89.7	82.1	85.9
4	709	35	93.6	90.8	82.2	82.0
5	950	45	99.4	99.4	97.5	97.1
6	850	49	99.1	98.7	97.9	97.6
7	850	35	98.3	98.3	96.5	96.6
8	850	21	96.9	95.6	89.6	95.0
9	950	25	99.4	99.1	95.7	97.3
10	1200	35	99.9	99.9	98.2	97.9

applied for 20 s; the two diagonals of the indent were measured and averaged to give a value for the indent diameter. Each sample was indented with at least 10 points well away from the sample edges, and with each indent being at least three diameters from the next indent, to allow an average value of hardness to be obtained.

The content of oxygen and nitrogen was measured before and after SPS processing using the inert gas fusion method with an ELTRA O/N 900; additionally, carbon content was found using the combustion method with an ELTRA C/S 800.

Results

Table 1 summarises the materials that have been used in this study. The spherical morphology, produced via gas atomisation (GA), can be seen in Fig. 3a, c, and i with a small percentage having a spherical internal pore that is an artefact of the production process. The angular powder is produced by the hydride-dehydride (HDH) process. These particles are angular with a largely irregular shape, due to being produced by crushing of scrap, swarf, and billet offcuts, see Fig. 3b and d. Material produced by the Metalysis process is spongy in nature with internal porosity in the particles; rutile ore is naturally angular and thus becomes both angular and spongy, see Fig. 3f. This porosity can be removed through a spheroidisation process to give spherical particles similar to those produced via GA, see Fig. 3e. Pigment-derived powder is again porous after the Metalysis process and the morphology is dependent upon the TiO_2 preform shape before the reduction; approximately spherical beads 1–2 mm in diameter, see Fig. 3g, or much smaller angular granules, see Fig. 3h, were used in this work.

Figure 3 shows the starting microstructures of the powders before sintering. The spherical GA particles show microstructures expected when rapidly cooling from the liquid phase; the Ti-6-4 and Metalysis spheroidised rutile-derived alloy show very fine acicular laths of martensite, the CP–Ti shows a variety of α grain sizes all smaller than the powder particles with some twinning visible. The CP–Ti HDH powder also shows a wide α grain size distribution and morphology within the particles and has more twinning within the grains. Ti-6-4 HDH has approximately equiaxed α grains surrounded by a very fine matrix of β at the α grain boundaries. The particles appear to exhibit two length scales of microstructure; some particles have α grains larger than 10 μm, whilst others have much finer α grains. Metalysis angular/spongy rutile shows a similar microstructure to Ti-6-4 HDH with α grains surrounded by a β matrix, although the α grains are less regular in size and shape. The pigment-derived alloy contains a similar microstructure in both morphologies with sub 50 μm equiaxed α grains present in the angular/spongy particles and slightly smaller more twinned α grains in the spherical/spongy particles, although the high porosity makes it difficult to assess.

Figure 4 shows details of the PSD of the alloy powders, with further analysis shown in Table 1; Dx (10), Dx (50), and Dx (90) are the diameters that 10, 50, and 90 % of particles are smaller than, respectively. The relative span is a measure of the distribution width about the median calculated by subtracting the Dx (10) value from the Dx (90) value and then dividing by Dx (50) value; the smaller the value the tighter the distribution. The spherical CP–Ti and Ti-6-4 have almost identical PSD with 80 % of the particle diameters being between 50 and 100 μm around a 70 μm median giving a relative span of 0.70 and 0.73, respectively. The HDH CP–Ti and Ti-6-4 are quite different in

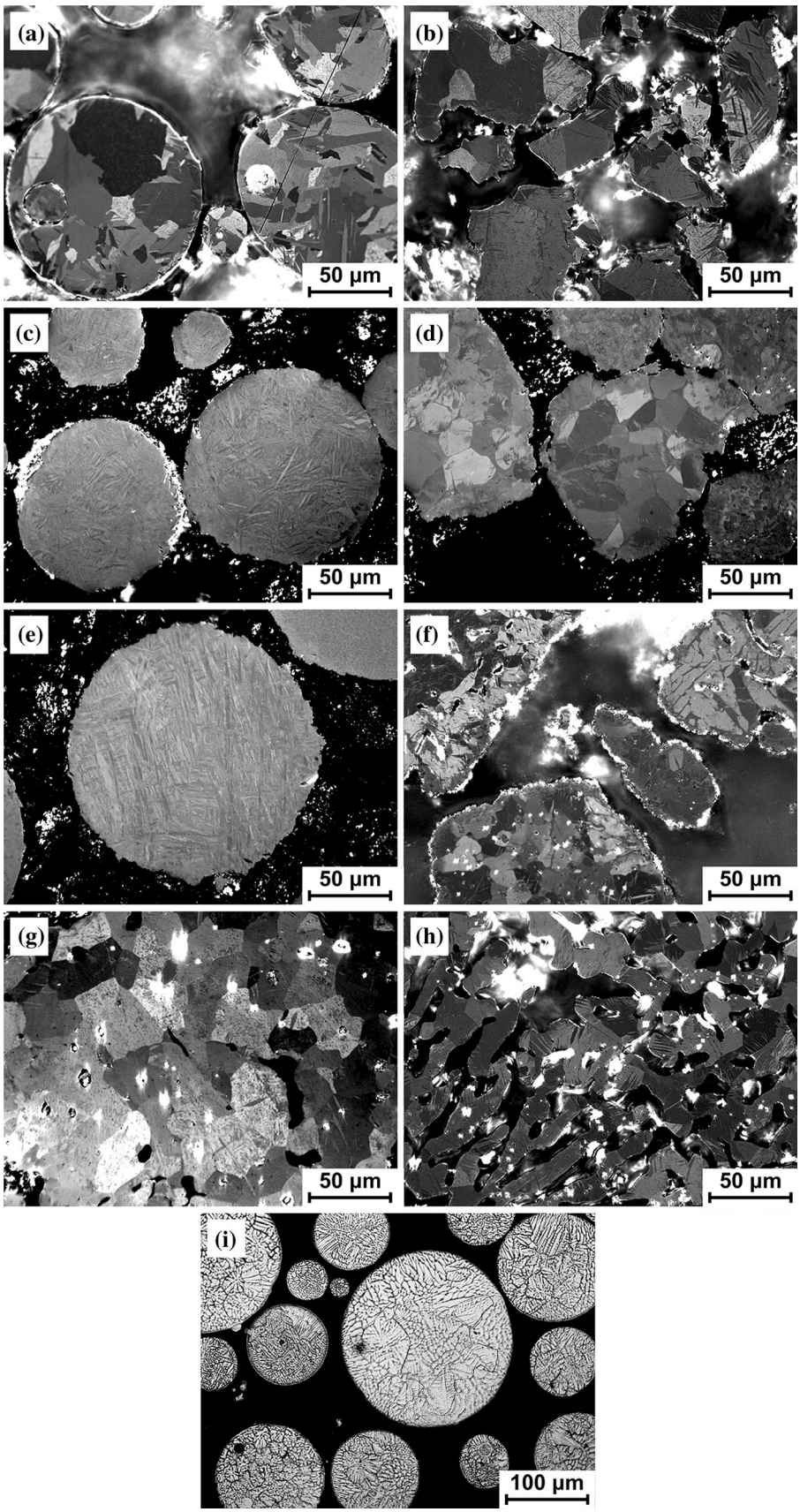

Fig. 3 Cross-polarised light micrographs illustrating particle size, morphology, and microstructure of the studied titanium alloy powders: **a** GA CP–Ti, **b** HDH CP–Ti, **c** GA Ti-6-4, **d** HDH Ti-6-4, **e** Metalysis spheroidised rutile grade, **f** Metalysis angular/spongy rutile grade, **g** Metalysis angular/spongy pigment grade, **h** Metalysis spherical/spongy pigment grade, **i** GA Ti-5553

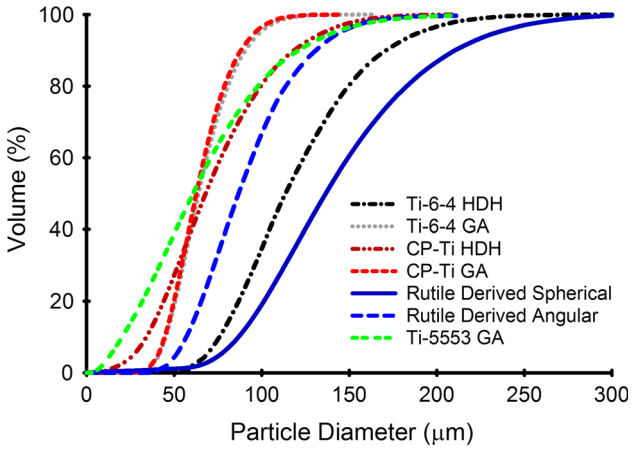

Fig. 4 Particle size distribution of the studied titanium alloy powders obtained by laser diffraction analysis

size but have a similarly shaped distribution, the middle 80 % of particles span approximately 100 μm but the CP–Ti is 50 μm smaller across the entire distribution meaning it has a larger relative span. The Ti-5553 was sieved to be <150 μm but was not sieved to have a minimum size, which is shown by a much lower Dx (10) and the greater span around the Dx (50). The Metalysis alloys were all provided sieved in particular size ranges; spherical rutile-derived alloy between 45 and 150 μm, spongy rutile-derived alloy between 75 and 250 μm, and angular/spongy pigment-derived alloy between 250 and 500 μm. These size fractions are carried through into the PSD with all three alloys having the middle 80 % within this range and a tight span around the median value. The spherical/spongy pigment-derived alloy was too large to put through the particle size analyser to get a PSD.

The D of E type approach showed for all four materials that pressure and temperature are proportional to density; increasing them causes increased final density. The increased pressure effects are most noticeable at the lower temperatures studied as the material does not achieve close to full density at these temperatures. Increasing the temperature is also more significant at the lower temperatures studied with the effect levelling off at higher temperatures as full density is approached. The densities and microstructures obtained from the central composite design study to investigate the effect of varying maximum temperature and pressure, whilst keeping a constant dwell period of 10 min and heating rate of 25°C min^{-1}, can be seen in Table 2 and Fig. 5. The microstructures in Fig. 5a,c, e, and g show the four materials after processing at 750 °C and 25 MPa, whilst b, d, f, and h show them after processing at higher conditions of 1200 °C and 35 MPa; these represent the lowest and highest densities achieved. Porosity is visible in the micrographs either as the darkest black or brightest white areas, due to either voids or colloidal silica from the final metallographic preparation stage crystallising in the voids. All four materials behave similarly with respect to a large increase in densification as the temperature and pressure are increased from the lowest to the highest values, with intermediate conditions causing intermediate densities. The GA CP–Ti increases from 90.5 to 99.9 %, the HDH CP–Ti from 89.7 to 99.9 %, the pigment derived from 82.1 to 98.2 %, and the rutile derived from 85.9 to 97.9 %. After processing at the lower temperature and pressure of 750 °C and 25 MPa, it is possible to see the outlines of the starting powders in all four materials, although it is most noticeable with the pigment-derived particles as they have large voids remaining at the interstices between particles and little of the internal porosity is removed. The rutile-derived alloy also retains voids between particles but these are much smaller at around 10–20 μm, and the internal porosity is again not removed. The GA and HDH CP–Ti have voids between particles similar in size to the rutile. After processing at 1200 °C and 35 MPa, there is almost complete removal of porosity from the GA and HDH CP–Ti; the porosity that remains consists of fine spherically isolated pores. The majority of large voids between particles are removed in both the pigment- and rutile-derived alloys. Homogeneously distributed small spherical pores remain in the rutile derived, whilst the distribution of small spherical pores in the pigment alloy is heterogeneous with areas of almost complete consolidation next to areas with significant porosity. Even at the lowest sintering temperature there is a significant change in microstructure from the starting particles. Recovery, recrystallisation, and grain growth are visible in all four materials, although it is most significant in the GA CP–Ti and least in the pigment-derived alloy due to the remaining porosity preventing grain growth. Figure 5a shows the GA CP–Ti grain structure has changed to more equiaxed slightly enlarged α grains after sintering at 750 °C and Fig. 5b shows that the higher temperature causes extensive grain growth, with some of the largest grains having dimensions in the order of several hundreds of microns. The HDH CP–Ti retains a smaller grain size than the GA powder at all processing conditions, as seen in Fig. 5c and d, there is a larger variation in grain size at 750 °C than with the GA CP–Ti and grain growth is observed to a lesser extent with many grains remaining <100 μm in diameter. The rutile-derived alloy has an inhomogeneous distribution of grain size at the lower temperature see Fig. 5e, which is also seen in the powder (Fig. 3), but after sintering at 1200 °C, Fig. 5f, the microstructure becomes finer and more homogeneous. The pigment-derived alloy retains the

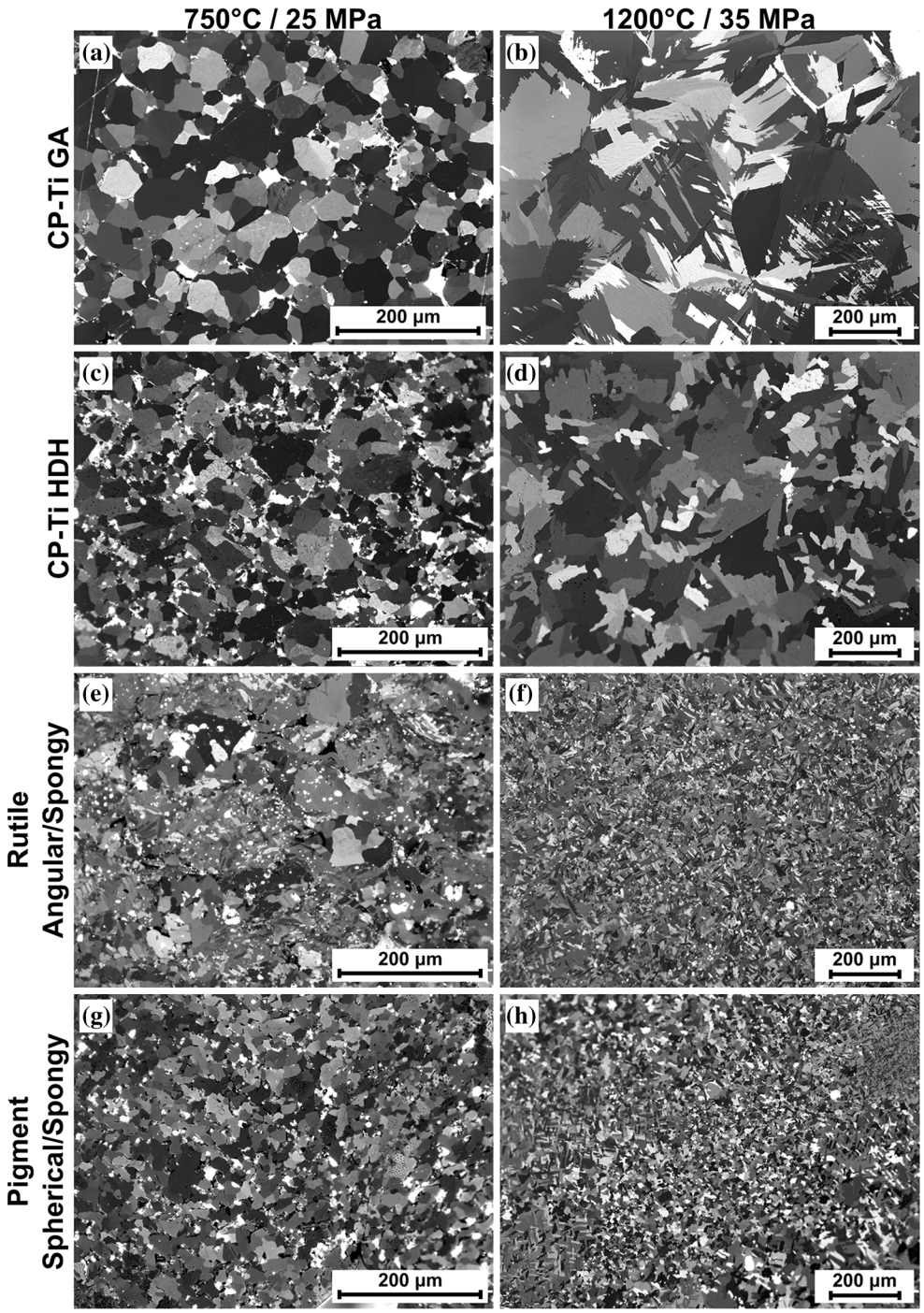

Fig. 5 Cross-polarised light micrographs showing microstructural development during constant heating rate and hold time SPS processing with varying hold temperatures and pressures for CP–Ti GA, CP–Ti HDH, Metalysis angular/spongy rutile grade, and Metalysis spherical/spongy pigment grade

microstructure from the starting particles at 750 °C, see Fig. 5g, but the microstructure becomes quite inhomogeneous at 1200 °C, see Fig. 5h, with areas of coarser and finer equiaxed α grains as well as areas of transformed β.

Figure 6 shows the data collected by the SPS machine during processing; the position of the hydraulic rams is measured continually from start position to finish position. As the starting density is known, and the final density was calculated as shown above, the relative density of the sample compared to 100 % dense can be graphed. The compliance of the machine has not been corrected for in these figures; as the start density is known and the final

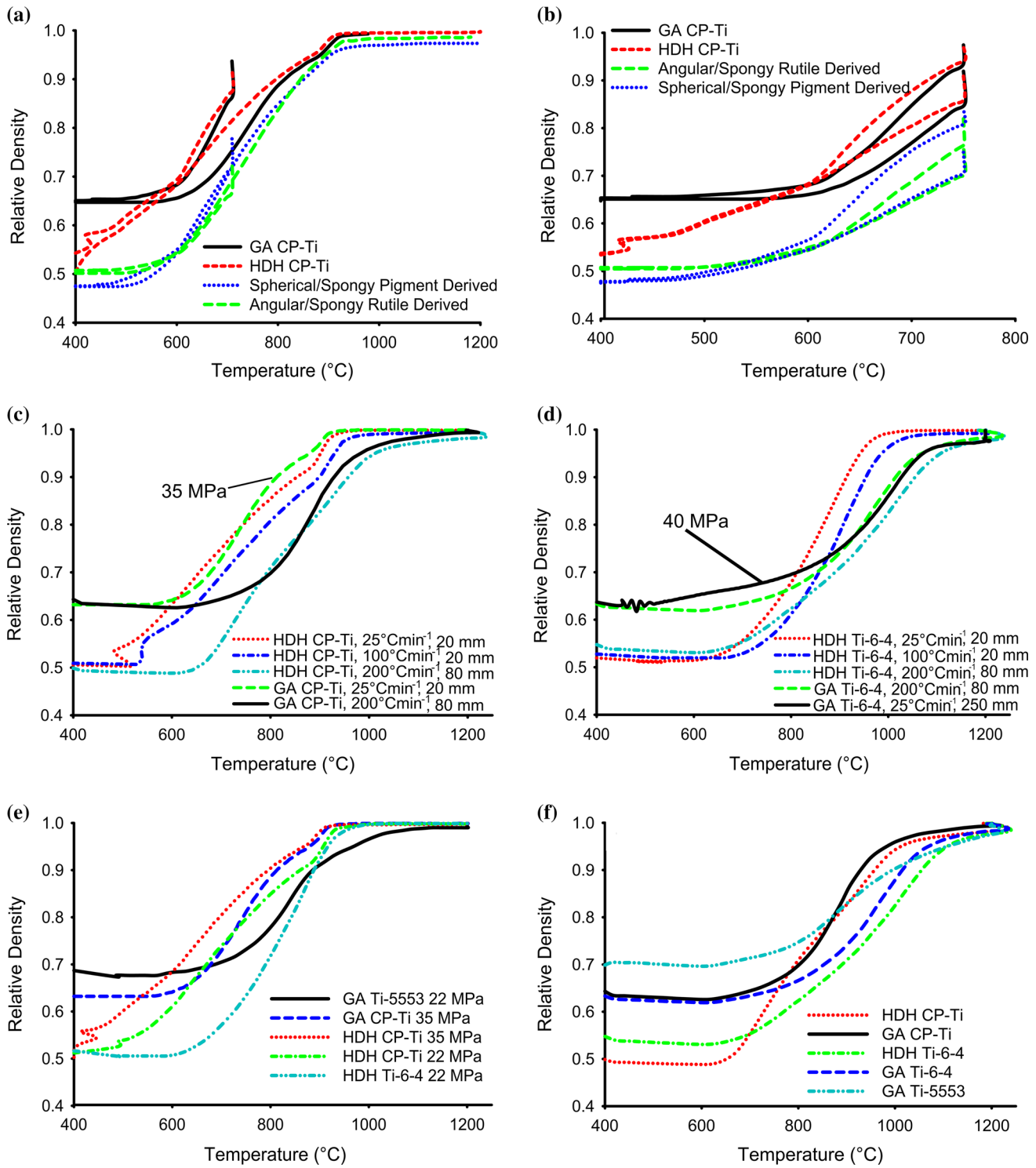

Fig. 6 SPS machine output data showing relative sample density against temperature during the process cycle (process conditions in each graph are equal unless otherwise stated or labelled): **a** Hold temperature increases from 709 to 1200 °C with 25°C min^{-1} heating rate, 35 MPa hold pressure, and 10 min hold time. **b** Hold pressure increases from 25 to 45 MPa with 25°C min^{-1} heating rate, 750 °C hold temperature, and 10 min hold time. **c** Heating rate increases from 25 to 200°C min^{-1} for HDH and GA CP–Ti with 1200 °C hold temperature, 22 MPa hold pressure, and 30 min hold time. **d** Heating rate increases from 25° to 200°C min^{-1} for HDH and GA Ti-6-4 with 1200 °C hold temperature, 22 MPa hold pressure, and 30 min hold time. **e** Change in morphology and chemistry with 1200 °C hold temperature, 25°C min^{-1} heating rate, and 30 min hold time. **f** Change in morphology and chemistry using 80-mm diameter moulds with 1200 °C hold temperature, 22 MPa hold pressure, 200°C min^{-1} heating rate, and 30 min hold time

density is calculated and then the whole data set is normalised with respect to full density the effect becomes negligible. Fig. 6a shows the difference between processing at 750 and 1200 °C. At 750 °C none of the alloys have reached full density and continue to compact during the dwell period. At 1200 °C, the CP–Ti reaches full density by 1000 °C and no further compaction occurs during the dwell; the Metalysis alloys behave similarly except that they only reach 98 % density and this does not increase during the dwell period. Figure 6b shows that increased pressure allows each alloy to consolidate more when the temperature is constant.

Figures 7, 8, 9, and 10 show the micrograph results from the heating rate and dwell study; all materials achieved over 99 % density using a hold temperature of 1200 °C and 21 MPa. The HDH CP–Ti in Fig. 7 shows an increase in prior β grain size, as well as an increase in α lath colony size, when the heating rate was increased from 25 to 100°C min^{-1}. There appears to be minimal difference in grain size between a hold time of 10 and 30 min at either heating rate. Figure 6c shows that the material compacts less for a given temperature when the heating rate is increased and this is also exacerbated by increasing the mould size used; this also holds true for GA CP–Ti. The HDH Ti-6-4 in Fig. 8 also shows little discernible difference in grain size or morphology when the hold time is increased but does show an increase in grain size when heating rate is increased. Figure 6d shows the same pattern repeated as described for HDH CP–Ti, and also shows the curve for the 250 mm 5 kg GA Ti-6-4 sample, which appears similar to the 80 mm GA Ti-6-4 curve, although has a lower heating rate and double the applied pressure. The spheroidised rutile-derived alloy in Fig. 9 shows little difference in microstructure when the heating rate is varied from 50 to 200°C min^{-1}, but there is a small increase in prior β grain size when the hold time is increased from 10 to 60 min. The GA Ti-5553 in Fig. 10 also shows little increase in grain size from 25–100°C min^{-1} heating rate and a small increase in grain size from 10–30 min hold time. Figure 6e shows the alloys displaying the same pattern of consolidation as seen in the hold temperature and pressure study, but also demonstrates how the chemistry effects compaction when the morphology is constant. Ti-6-4 HDH achieves much lower densities at equivalent temperature than CP–Ti HDH and does not display the same linear initial consolidation. Whilst Ti-5553 has the highest initial density it is the last alloy to finish consolidating. Finally Fig. 6f shows that the same patterns of consolidation are displayed when the process is scaled up from 20 to 80-mm diameter moulds; the Ti-6-4 compacts less for a given temperature than CP–Ti and rutile-derived powder lies between them. Ti-5553 again shows a much slower rate

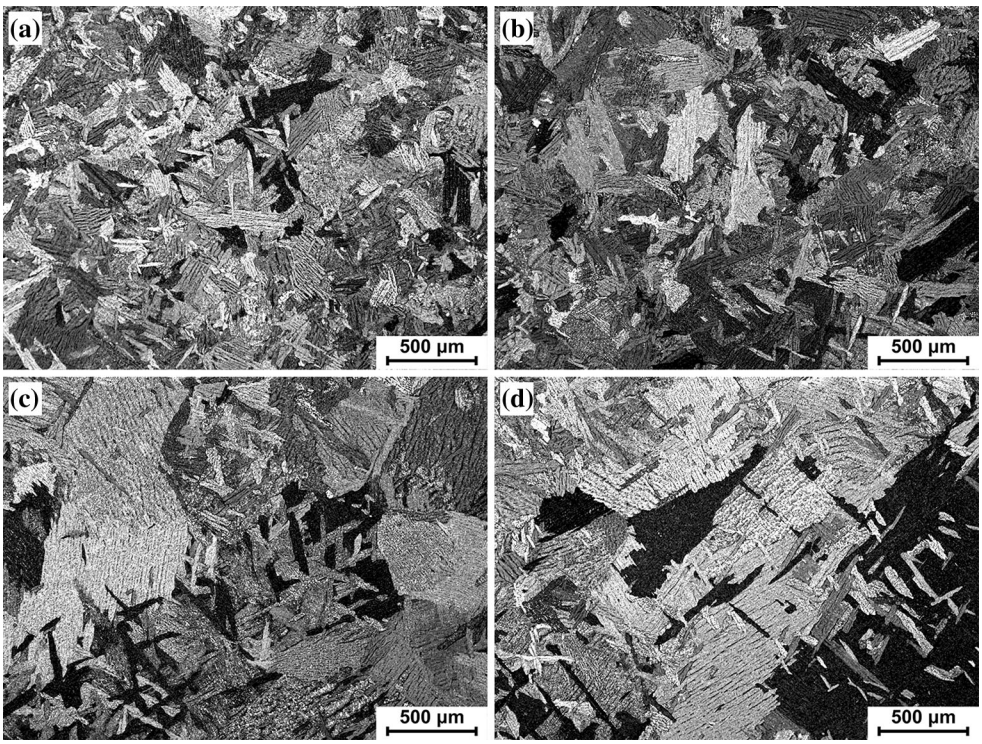

Fig. 7 Light micrographs showing microstructural development of CP–Ti HDH powder during SPS processing at 1200 °C/35 MPa, with varying heating rate and hold time: **a** 25°C min^{-1}/10 min, **b** 25°C min^{-1}/30 min, **c** 100°C min^{-1}/10 min, **d** 100°C min^{-1}/30 min

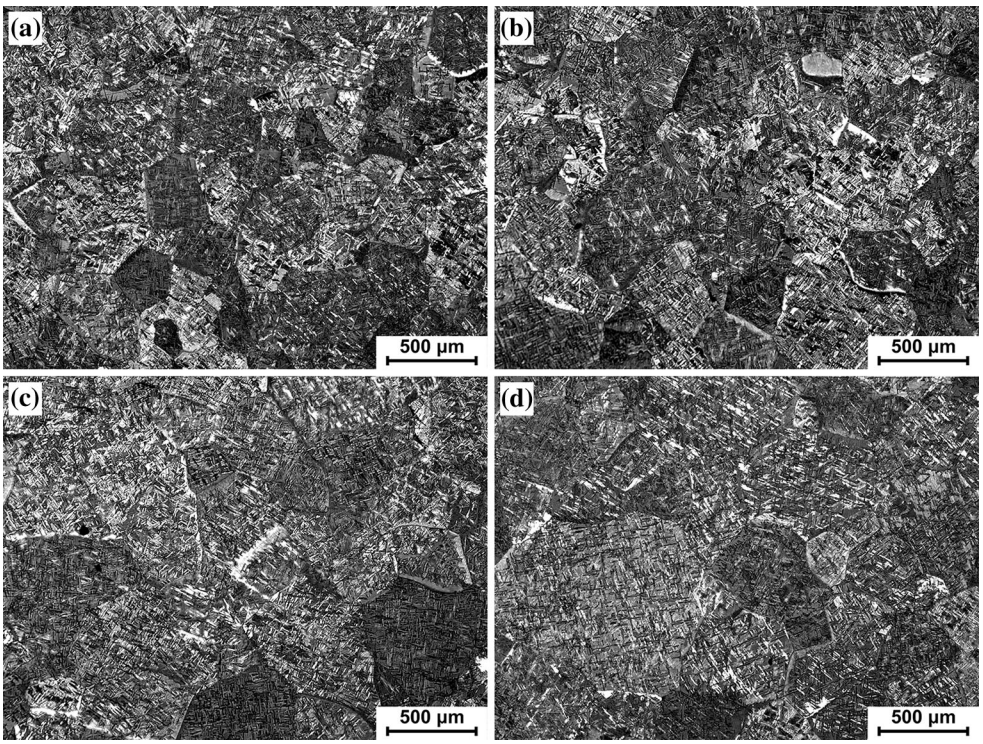

Fig. 8 Light micrographs showing microstructural development of Ti-6-4 HDH powder during SPS processing at 1200 °C/35 MPa, with varying heating rate and hold time: **a** 25°C min^{-1}/10 min, **b** 25°C min^{-1}/30 min, **c**100°C min^{-1}/10 min, **d** 100°C min^{-1}/30 min

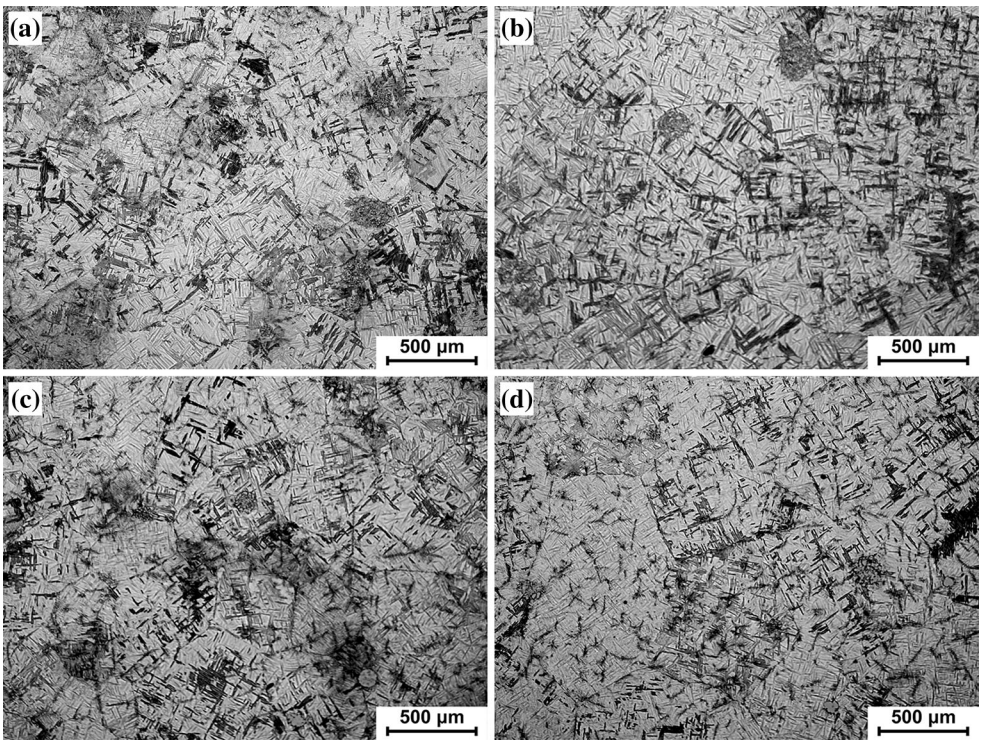

Fig. 9 Light micrographs showing microstructural development of Metalysis spheroidised rutile grade powder during SPS processing at 1200 °C/35 MPa, with varying heating rate and hold time: **a** 50°C min^{-1}/10 min, **b** 50°C min^{-1}/60 min, **c** 200°C min^{-1}/10 min, **d** 200°C min^{-1}/60 min

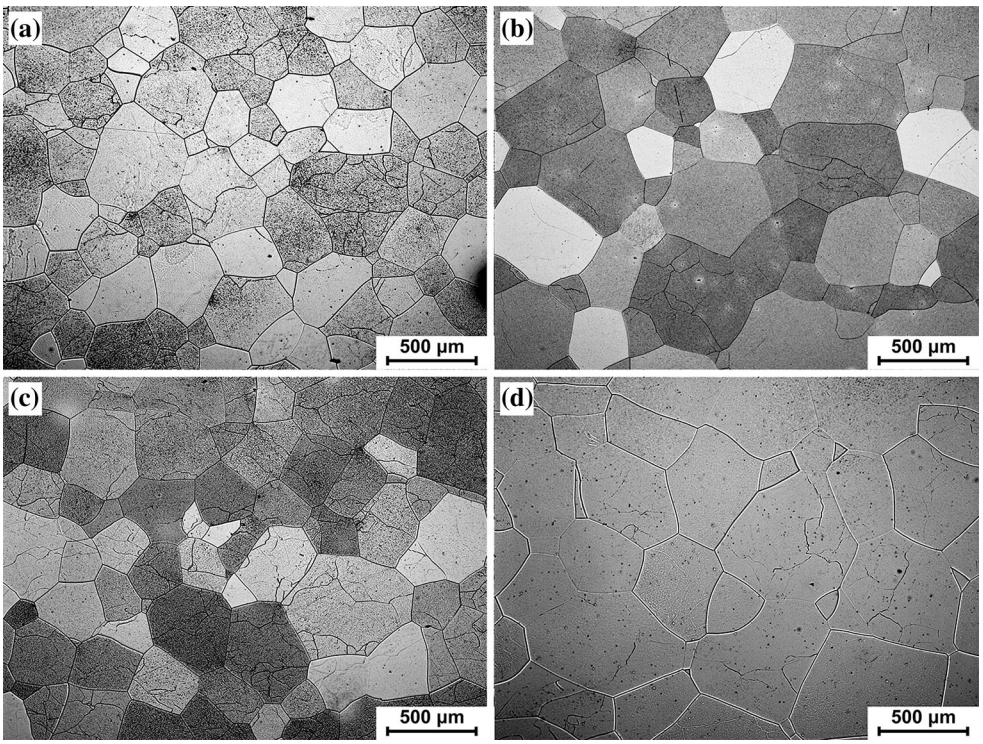

Fig. 10 Light micrographs showing microstructural development of Ti-5553 GA powder during SPS processing at 1200 °C/35 MPa, with varying heating rate and hold time: **a** 25°C min^{-1}/10 min, **b** 25°C min^{-1}/30 min, **c** 100°C min^{-1}/10 min, **d** 100°C min^{-1}/30 min

of consolidation. All alloys overshoot the hold temperature and continue to consolidate during this period, but appear to reach full density before the dwell period begins.

Figure 11 shows the microstructure produced across the radius of the 250-mm diameter SPS disc. It can be seen from the centre in Fig. 11a to the edge in Fig. 11e that the microstructure remains comparable; the prior β grain size, α lath colony size, α lath thickness, and grain boundary α all remain consistent. The density also remains constant with 99.99 % found at all five positions.

The oxygen, carbon, and nitrogen content of the GA CP–Ti, GA Ti-6-4, spheroidised rutile derived and angular pigment derived, were measured before and after SPS with the levels shown in Table 3. The material was processed at 1200 °C under 21 MPa with a heating rate of 200 °C/min and a hold time of 60 min. The CP–Ti was within specification for interstitial content (800 ppm C, 300 ppm N, 2500 ppm O) as powder and remained within specification after SPS processing apart from nitrogen. The Ti-6-4 also remained within specification after SPS processing (800 ppm C, 500 ppm N, 2000 ppm O). The Metalysis alloys also experienced minimal interstitial pick-up during SPS processing. The average interstitial pick-up after SPS processing was 150 ppm additional to the starting level, excluding the carbon level in the rutile that appeared to drop. It should be noted that the supplied Metalysis alloy powders are still at the development stage and so have slightly elevated interstitial content. Table 3 also shows the Vickers hardness value for the alloys after SPS. The CP–Ti and Ti-6-4 have values very close to conventionally processed material, whilst the hardness values of the Metalysis alloys lie between the two commercial grades.

Discussions

Influence of powder morphology and size on consolidation behaviour

The effect of hold temperature and pressure

Each material tested behaves in broadly the same way when exposed to varying hold temperatures and pressures; as the hold temperature and pressure are increased there is a corresponding increase in density, as seen in Figs. 5, 6a, and b. The effect of increased pressure on consolidation is most noticeable at 750 °C when the samples do not attain full density and is much less when using a hold temperature of 991 °C or above. When the temperature reaches 600 °C, the pressure begins to increase, for lower hold pressure the increase is more gradual than for higher hold pressure; therefore processing with higher set hold pressure causes

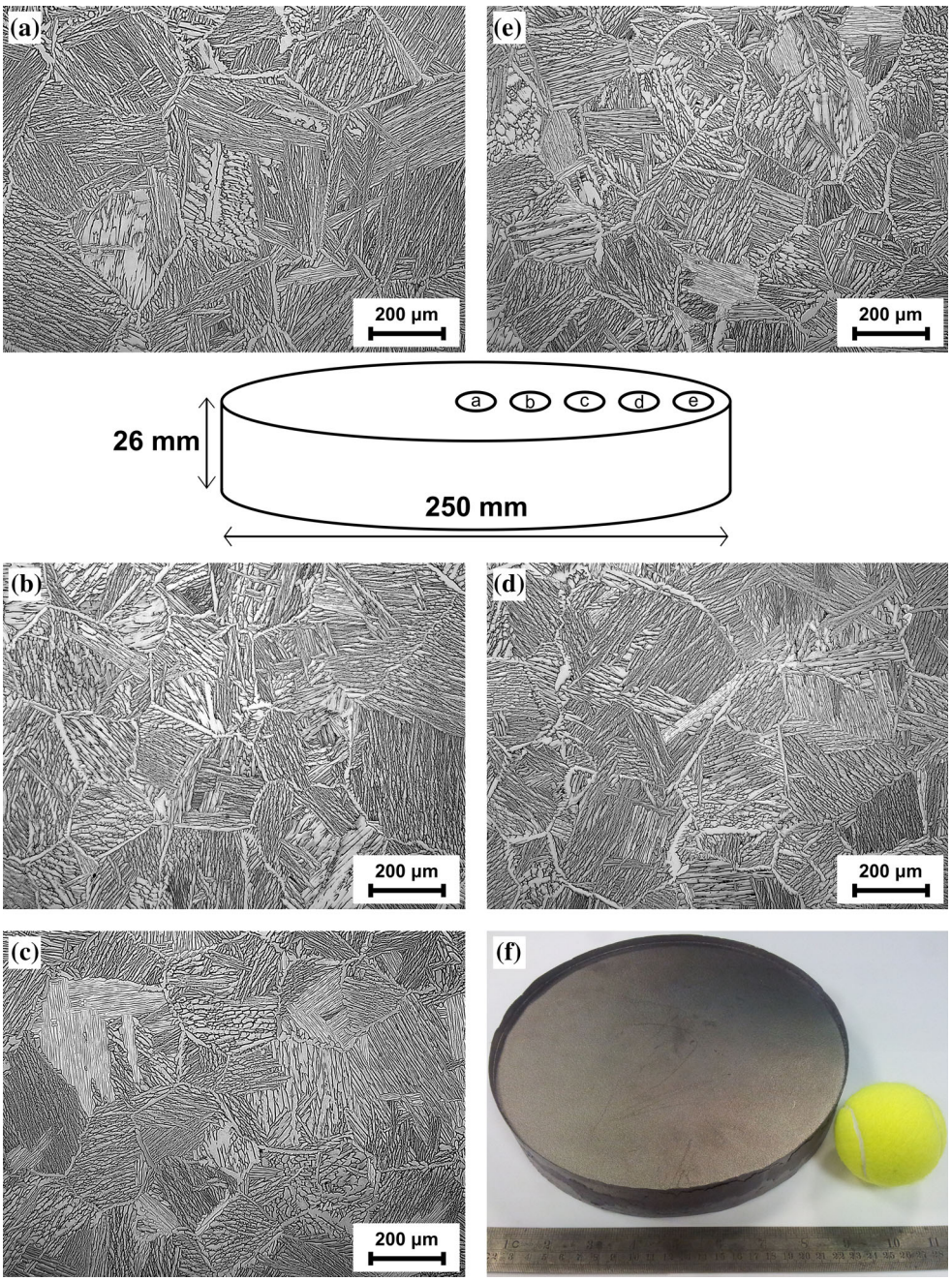

Fig. 11 Light micrographs showing microstructures from the centre **a** to the edge **e** of 25-mm diameter Ti-6-4 SPS disc. Photograph of 250-mm diameter SPS disc **f**

faster initial consolidation. This is due to the material having higher flow stress at lower temperatures so more force is needed to overcome this and cause plastic flow of the particles to allow consolidation. Although higher pressure earlier in the cycle gives more rapid consolidation, if the temperature is increased enough the lower pressure can still achieve full density due to the continuing decrease in material flow stress. At higher temperatures the effects of diffusion controlled sintering mechanisms also become more significant, aiding removal of remaining porosity. Of interest is the behaviour of the HDH and GA CP–Ti, which have identical chemistry and differ only in the particle size and morphology, see Figs. 3 and 4. The HDH powder is more irregularly shaped and has a wider size distribution, it processes to a smaller grain size at all tested conditions and a reduction in density at conditions that do not produce full consolidation, see Fig. 5. It was initially thought that the cause for this was the packing density of the angular HDH powder being 54 %, which is less than that of the spherical GA powder at 65 %. However, this difference in density is

Table 3 Nitrogen, oxygen, and carbon content analysis and Vickers hardness values for four materials pre- and post-SPS

Chemistry	Morphology	Carbon (ppm)	Oxygen (ppm)	Nitrogen (ppm)	Vickers hardness	ASTM Vickers
CP-Ti	Spherical Powder	34	1204	121	168	~150
	Post-SPS	238	1440	336		
Ti-6-4	Spherical Powder	153	1487	252	340	~350
	Post-SPS	266	1585	394		
Pigment derived	Angular/spongy Powder	1036	3084	31	258	N/A
	Post-SPS	1169	3293	98		
Rutile derived	Spherical Powder	3830	3232	175	281	N/A
	Post-SPS	3463	3295	358		

rapidly overcome in the initial stages of the process, see Fig. 6a. The HDH powder undergoes a significant amount of compaction before 600 °C increasing to approximately 70 % density, whereas during this initial part of the cycle the GA powder compacts very little from the 65 % starting value. The angular nature of the HDH particle contacts acts to concentrate the applied stress more than the circular GA particle contacts, there are also fewer contacts as the porosity is higher again increasing the effective stress. This increase in effective stress allows earlier consolidation by plastic flow as the yield stress is exceeded. The GA morphology densifies more during the hold period than the HDH, often achieving a higher final density after the complete cycle. This can be seen by the much larger grain sizes found in the GA powder, the removal of pores allows increased grain boundary motion and therefore grain growth; the assumption is that removing the final remaining pores from the HDH samples is more difficult and they continue to prevent grain growth. The regular spherical nature of the particles and grains within the GA material are also more stable as they have the lowest surface energy per unit volume and therefore grow more easily. Plastic flow is clearly more effective for consolidating HDH powder earlier in the cycle, but after the particle contacts become large enough that the effective stress falls below the flow stress diffusion mechanisms are more effective in the final removal of porosity with the GA morphology.

The larger variation in grain size experienced by the HDH powder can also be explained by the more random packing. Areas with higher initial particle-to-particle contacts and smaller pores will undergo more densification than areas with less particle interactions and larger pores; once the powder has densified, the porosity stops pinning the grain boundaries and allows grain growth to occur which gives areas of differing grain size. It would appear that the GA powder reaches a stage where enough porosity is removed to allow grain boundary motion and grain growth before HDH powder does, thus allowing HDH powder to retain a smaller grain size when processed to full density. Whilst difficult to directly compare to CP–Ti due to significantly different chemistries, the Metalysis alloys' sintering behaviour fits between that described for the HDH and GA, although both densify less for the same processing conditions possibly due to the spongy nature of the particles with internal porosity being retained, see Fig. 5. They both show some initial densification between 470–600 °C; see Fig. 6b, most likely due to a similar mechanism to the HDH. The highly porous nature amplifying applied stress, and larger scale, of the spherical pigment particles means there are much larger voids for initial particle repacking and deformation to give more rapid consolidation than the rutile alloy. The rutile- and pigment-derived alloys show the same areas of more rapid grain growth as the HDH, which could also be explained by the same mechanism. The spherical/spongy pigment alloy is an order of magnitude larger than the spherical GA particles and this can be seen by the large remaining pores at interstices between the particles at lower temperatures and pressures; these pores take much longer to remove via heat-activated sintering mechanisms and therefore the conditions with the highest pressure but mid-temperature achieved the highest density, see Table 2, as the pressure and therefore plastic flow is more significant on the larger length scales involved with this morphology. The pigment alloy retains an inhomogeneous microstructure after sintering at 1200 °C; some areas have a transformed β structure suggesting cooling from above the β transus whilst others retain a recrystallised equiaxed α structure. A cause could be that there is some

chemical inhomogeneity between particles in the starting material that is not dispersed during processing due to the larger length scales involved with this morphology; some areas do not go above their local β transus and remaining porosity prevents significant grain growth by pinning grain boundaries, which is possible as the measured density is 97.5 %. This ties in with the approximate size of the areas of differing microstructure corresponding to starting particle size. At 1200 °C the rutile has gone above the β transus temperature allowing β grain growth, and an increased prior β grain size, but giving finer more homogenous transformed β α colonies after cooling.

The effect of varying hold time and heating rate

Hold time and heating rate have been shown to have minimal effect on final density, and varying effect on grain size and structure, in the range studied, see Figs. 7, 8, 9, 10, and 11. The temperatures and pressures used to study the effect of hold time produced full consolidation at the shortest time and therefore increasing the time had no measurable effect on density. However when the conditions used do not attain full consolidation then a dwell period allows further densification to occur, as seen in the hold temperature and pressure study, see Figs. 6a and b. For the HDH morphology, with both CP–Ti and Ti-6-4, an increase in heating rate causes the material to densify less at a given temperature, see Figs. 6c and d. Typically the slower heating rate achieved greater consolidation at a given temperature but took longer to reach that temperature. It is important to note that whilst using higher heating rates gives less consolidation at a given temperature, when compared to equivalent time elapsed in the processing cycle the higher heating rates produce significantly higher densities. The lag in consolidation may be explained by the higher heating rate causing thermal gradients in the sample, meaning some of the material would not consolidate as fully until thermal equilibrium is reached in the hold period. Another explanation may be viscoplastic effects; the higher heating rates are accompanied by more quickly applied pressure, leading to more rapid consolidation that may cause an increase in material flow stress and retard further densification. Other than a decrease in density at a given temperature the heating rate does not affect how the material consolidates.

Influence of chemistry on consolidation

The effect of varying hold temperature and pressure

Diffusion processes are key in sintering and when a titanium alloy undergoes the α to β phase transformation there is a large increase in diffusivity; self-diffusion of Ti in the β phase is approximately three orders of magnitude higher than in the α phase. This can be seen when the sintering temperature is taken above the β transus temperature as there is a marked increase in densification rate. This is seen quite obviously for the GA and HDH CP–Ti in Figs. 6a, c, and 7e, and to a lesser extent the pigment-derived alloy, at around 890 °C. This is approximately 20 °C lower than might be expected, but as the pyrometer reads off the outside of the graphite mould this difference could easily be expected. There is no obvious increase in densification rate for the rutile-derived alloy suggesting a high β transus temperature, which may be due to the alloying elements or higher than desirable interstitial levels. However, the microstructure produced after sintering at 1200 °C would suggest that the alloy has gone over the β transus temperature as there has been a homogenisation of grain size and shape, meaning that the α visible is likely transformed from prior β grains. The alloy chemistry affects the way the material densifies; when hold temperature/pressure, heating rate, and particle morphology are kept constant. As described, the HDH morphology and CP–Ti chemistry show a period of almost linear consolidation rate up to 600 °C followed by a rapid rate increase that reduces exponentially, with a further rate increase if the β transus is surpassed, see Fig. 6a. However, for the same morphology and conditions but Ti-6-4 chemistry the material consolidates differently; with little densification occurring until 600 °C followed by the rapid rate increase exponentially reducing as full density is approached, see Fig. 6d, much like the CP–Ti GA morphology described in the hold temperature/pressure study. Furthermore, the increase in consolidation when the β transus is reached is not seen with Ti-6-4, although this may be due to almost full consolidation being achieved by the time the transus temperature is reached so the increase is not noticeable. The Ti-5553 GA also shows no increase in consolidation at its much lower β transus temperature, which could be due to the rapid densification already occurring due to plastic flow making the increase in diffusion insignificant. Regardless of the particle morphology, the same pattern is seen during sintering when comparing the chemistries. For the HDH morphology, the CP–Ti consolidates more rapidly than Ti-6-4, which is mirrored with the GA morphology. This is likely due to the increased flow strength of the Ti-6-4 at elevated temperature preventing particle deformation by plastic flow, which is supported by the rutile-derived spheroidised alloy consolidating in an intermediate way between CP–Ti and Ti-6-4. This fits in with the hardness values obtained for the three materials after SPS processing, which estimates the yield strength of the rutile alloy to be between CP–Ti and Ti-6-4, see Table 3.

The effect of varying hold time and heating rate

The effect of hold time and heating rate on the microstructure after sintering is more inconclusive. With a constant hold temperature and pressure, and the HDH morphology, it is possible to compare CP–Ti with Ti-6-4. Increasing the heating rate from 25 to 100°C min^{-1} gives an increase in prior β grain size, but an increased hold time does not increase the grain size at either heating rate, see Figs. 7 and 8. It appears somewhat counterintuitive that the increased heating rate should increase the grain size as the alloy will spend less overall time at higher temperatures with a quicker heating rate. However, this may be down to the rapid heating rate bypassing the traditional initial stages of sintering where a network of interconnected pores is created and then broken up, trapping closed pores within the material and preventing grain growth. At high heating rates, the particles quickly become very soft and thus deform rapidly under the applied load. Particle deformation and rearrangement to fill voids could drastically reduce the trapped porosity within the material and thus allow grain growth to occur during the hold period. The reason grain growth appears not to increase during the hold period could be that the initial rapid grain growth expected at such high temperature has already occurred after 10 min and little additional growth is noticeable after an extra 20 min. Conversely with the spherical morphology there seems to be little increase in prior β grain size with increasing heating rate for either chemistry, but a small increase in prior β grain size with increased hold time, see Figs. 9 and 10. It is unclear why the spherical particles do not follow the same increase in grain size with increased heating rate as angular particles other than the already suggested mechanism, whereby angular HDH powder amplifies the applied stress causing more rapid initial consolidation bypassing the initial stages of sintering, not having as much effect with the larger spherical particle contacts.

Influence of mould size on consolidation

When the mould size used is increased there is a large reduction in consolidation at a given temperature compared to a smaller mould, see Fig. 6d. If the mould diameter is doubled then the mass of powder to produce the same thickness of sample is quadrupled. This increase in powder mass means there is more likely to be thermal gradients induced in the sample, and therefore all the material will not be at the temperature measured by the pyrometer. This consolidation lag is eliminated, or almost so, by the time the hold temperature is reached, if this corresponds to full density. Due to the increased thermal mass of the larger samples, there is usually an overshoot of hold temperature and by the time this overshoot corrects the same density is achieved as for smaller moulds; for the largest 250-mm diameter mould used this was not the case and densification continued during the hold period. It is worth noting that the slower heating rate and increase hold pressure allowed the 250-mm diameter mould to match the 80-mm mould for consolidation when Ti-6-4 GA powder was used, which supports the theories proposed above. The microstructure was found to be consistent throughout samples when using the smaller diameter moulds and importantly this translates to the much larger diameter mould used, see Fig. 11. This suggests that if thermal/pressure gradients, or current flow inhomogeneity, do exist within the sample that they do not have an impact upon density or microstructure, or that the dwell period used allows homogenisation to occur.

The oxygen, carbon, and nitrogen analysis gives a good indication as to the suitability of SPS processing for consolidating powder. The argon and vacuum combination appears to have provided an atmosphere where few interstitials are picked up during the processing, see Table 3. The carbon pick-up is unsurprising as the mould, which is in contact with the powder, is made of graphite. It could be possible to further reduce the carbon pick-up by insulating the faces of the mould to provide a barrier between the carbon and powder, however, care would need to be taken so as not to prevent the electric current flowing. The oxygen and nitrogen pick-up must come from remaining atmosphere in the vacuum chamber and would be more problematic to remove if lower levels were required, although improving the level of vacuum should help. It should also be noted that interstitial pick-up is highest at the edges of the sample and therefore depending upon the next processing step that the increases reported here may not be an issue, especially if a finish machining step were to remove the outer layers or additional thermomechanical processing was to occur.

Conclusions

This work has shown that the processing of titanium alloy feedstock via spark plasma sintering is a viable method of consolidation, and that when combined with potentially low-cost powders from alternative extraction methods and precision forging; it could contribute to a disruptive technology. The process is tolerant of input material, especially when conditions are used that produce full consolidation; materials may initially consolidate at different rates but will reach full density regardless.

The hold temperature and pressure are the most significant process parameters when attempting full consolidation of titanium alloy powders. The highest pressure possible should be used and the experience in this study is that the strength of the graphite ring mould will be the

limiting factor. Higher temperatures produced higher densities with other factors equivalent, and titanium alloy powders should be heated above the β transus temperature to take advantage of the higher diffusion rates. The heating rate offered no advantage in increasing density for the processing conditions used as they all produced full consolidation; although a small increase in grain size is measured with increased heating rate. This increase in grain size is probably acceptable due to the reduction in process cycle time possible by higher heating rates, especially if a further thermomechanical processing is to be performed. The dwell period is necessary to achieve full density if it has not been reached during the heating part of the cycle; this becomes more necessary as the mass of powder and/or size of mould are increased. At the 20 mm diameter, tens of grams level, increasing the dwell time from 10 to 60 min does not increase the density and slightly increases grain size. As the mass of powder to be sintered increases so do the power requirements to achieve the higher heating rates, the 80-mm diameter moulds with approximately 300 g of powder were at the limit of the power supply for the type HP D 25 SPS furnace used in the study. It may not be possible to heat large amounts of titanium powder at the highest heating rates in the current generation of SPS furnaces; however, as discussed, the work by Chennoufi et al. [14] may alleviate some of these problems by reducing the current and power requirements by replacing the all graphite SPS mould assemblies.

The smaller the feedstock size, the easier it is to achieve full consolidation due to the smaller length scales involved, although it is still possible to fully consolidate larger particles via SPS. Angular or spherical powder particle morphology also has little impact on final density, although a smaller grain size can be retained with an angular morphology. Particles with internal porosity present greater difficulty to process to full consolidation under the conditions studied. The spongy Metalysis material only reached 98 % density compared to the 99.9 % of GA or HDH morphology; it is believed that increased pressure and hold time would allow the final 2 % of porosity to be removed. When the rutile is spheroidised to remove the particle porosity the resulting spherical particles consolidate in the same fashion as GA powder, showing that the rutile-derived chemistry is not the issue rather the spongy particle morphology. Processing is also affected by alloy chemistry with the varying β transus temperatures and high temperature flow stresses all changing the ease of full consolidation. For example, CP–Ti which has the lowest flow stress of the alloy powders tested was the first to achieve full consolidation.

A 5 kg 250-mm diameter disc was successfully produced via SPS, demonstrating that the process and technology can economically be scaled up to produce real world parts. The microstructures produced via SPS do not lend themselves to the properties required for finished titanium products and therefore a further thermomechanical finishing step should be applied to produce components of near net shape with competitive mechanical properties. No discernible difference in microstructure or density was found throughout the 250 mm sample and this finding suggests the use of SPS on an industrial scale is feasible; a finishing forging step does not need to account for microstructural inhomogeneity throughout the preform billet. This processing route could be utilised to produce valve springs for car engines or parts for landing gear assemblies; giving the well-known benefits of high strength titanium alloys to these applications but at a significant cost reduction.

To further this work, a study will be undertaken to assess the SPS consolidated titanium alloys under forging conditions. A processing window will be established to allow a one-step forge to be applied to SPS preforms to produce finished components.

Acknowledgements The authors acknowledge the Engineering and Physical Sciences Research Council's Advanced Metallic Systems Centre for Doctoral Training for funding Nick Weston. The authors thank the Defence Science and Technology Laboratory for additional funding and Dr. Matthew Lunt for useful discussions. The authors would like to acknowledge Dr. Akemi Nogiwa-Valdez for technical assistance with the SPS furnace. Finally, the authors acknowledge Metalysis Ltd. for supply of material and Dr. Kartik Rao and Lucy Grainger for useful discussions.

References

1. Kraft EH (2004) Summary of emerging titanium cost reduction technologies. Report by ehk technologies, Vancouver, WA. Study for US DofE and ORNL/Subcontract 4000023694
2. Hurless BE, Froes FH (2002) Lowering the cost of titanium. AMPTIAC Q 6:3–9
3. Fray DJ (2008) Novel methods for the production of titanium. Int Mater Rev 53:317–325. doi:10.1179/174328008X324594
4. Chen G, Fray D, Farthing T (2000) Direct electrochemical reduction of titanium dioxide to titanium in molten calcium chloride. Nature 407:361–364. doi:10.1038/35030069
5. Mellor I, Grainger L, Rao K, Deane J, Conti M, Doughty G, Vaughan D (2015) Titanium powder production via the metalysis process. In: Qian M, Froes FH (eds) Titanium powder metallurgy: science, technology and applications, 1st edn. Elsevier, Amsterdam, pp 51–68
6. Jackson M, Dring K (2006) A review of advances in processing and metallurgy of titanium alloys. Mater Sci Technol 22:881–887. doi:10.1179/174328406X111147
7. Druz VA, Moxson VS, Chernenkoff R, Jandeska WF, Lynn J (2006) Blending an elemental approach to volume titanium manufacture. Met Powder Rep 10:16–21
8. Norgate TE, Wellwood G (2006) The potential applications for titanium metal powder and their life cycle impacts. JOM 58:58–63. doi:10.1007/s11837-006-0084-y
9. Froes FH, Mashl SJ, Moxson VS, Hebeisen JC, Druz VA (2004) The technologies of titanium powder metallurgy. JOM 56:46–48

10. Lutjering G, Williams J (2003) Titanium: engineering materials and processes, 2nd edn. Springer, Hiedelberg, pp 50–52
11. Eriksson M, Radwan M, Shen Z (2013) Spark plasma sintering of WC, cemented carbide and functional graded materials. Int J Refract Metals Hard Mater 36:31–37. doi:10.1016/j.ijrmhm.2012.03.007
12. Orrù R, Licheri R, Locci AM, Cincotti A, Cao G (2009) Consolidation/synthesis of materials by electric current activated/assisted sintering. Mater Sci Eng 63:127–287. doi:10.1016/j.mser.2008.09.003
13. Musa C, Licheri R, Locci AM, Orrù R, Cao G, Rodriguez MA, Jaworska L (2009) Energy efficiency during conventional and novel sintering processes: the case of Ti–Al_2O_3–TiC composites. J Clean Prod 17:877–882. doi:10.1016/j.jclepro.2009.01.012
14. Chennoufi N, Majkic G, Chen YC, Salama K (2009) Temperature, current, and heat loss distributions in reduced electrothermal loss spark plasma sintering. Metall Mater Trans A 40A:2401–2409. doi:10.1007/s11661-009-9934-x
15. Handtrack D, Despang F, Sauer C, Kieback B, Reinfried N, Grin Y (2006) Fabrication of ultra-fine grained and dispersion-strengthened titanium materials by spark plasma sintering. Mater Sci Eng 437:423–429. doi:10.1016/j.msea.2006.07.143
16. Sumida M, Kondoh K (2005) In-Situ synthesis of Ti matrix composite reinforced with dispersed Ti 5 Si 3 particles via spark plasma sintering. Mater Trans 46:2135–2141
17. Nicula R, Lüthen F, Stir M, Nebe B, Burkel E (2007) Spark plasma sintering synthesis of porous nanocrystalline titanium alloys for biomedical applications. Biomol Eng 24:564–567. doi:10.1016/j.bioeng.2007.08.008
18. Sakamoto Y, Moriyama S, Endo M, Kawakami Y (2008) Mechanical Property of Porous Titanium Produced by Spark Plasma Sintering. Key Eng Mater 385–387:637–640. doi:10.4028/www.scientific.net/KEM.385-387.637
19. He D, Fu Z, Wang W, Zhang J, Munir Z, Liu P (2012) Temperature-gradient joining of Ti–6Al–4V alloys by pulsed electric current sintering. Mater Sci Eng 535:182–188. doi:10.1016/j.msea.2011.12.061
20. Miriyev A, Stern A, Tuval E, Kalabukhov S, Hooper Z, Frage N (2013) Titanium to steel joining by spark plasma sintering (SPS) technology. J Mater Process Technol 213:161–166
21. Chaudhari R, Bauri R (2014) Microstructure and mechanical properties of titanium processed by spark plasma sintering (SPS). Metallogr Microstruct Anal 3:30–35. doi:10.1007/s13632-013-0112-6
22. Menapace C, Vicente N, Molinari A (2013) Hot forging of Ti–6Al–4V alloy preforms produced by spark plasma sintering of powders. Powder Metall 56:102–110. doi:10.1179/1743290112Y.0000000003
23. Eriksson M, Shen Z, Nygren M (2005) Fast densification and deformation of titanium powder. Powder Metall 48:231–236. doi:10.1179/174329005X71939
24. Zadra M, Casari F, Girardini L, Molinari A (2008) Microstructure and mechanical properties of cp-titanium produced by spark plasma sintering. Powder Metall 51:59–65. doi:10.1179/174329008X277000
25. Muñoz S, Anselmi-Tamburini U (2010) Temperature and stress fields evolution during spark plasma sintering processes. J Mater Sci 45:6528–6539. doi:10.1007/s10853-010-4742-7
26. Anselmi-Tamburini U, Garay JE, Munir ZA (2005) Fundamental investigations on the spark plasma sintering/synthesis process III. Current effect on reactivity. Mater Sci Eng 407:24–30. doi:10.1016/j.msea.2005.06.066
27. Munir ZA, Quach DV, Ohyanagi M (2011) Electric Current Activation of Sintering: a Review of the Pulsed Electric Current Sintering Process. J Am Ceram Soc 94:1–19. doi:10.1111/j.1551-2916.2010.04210.x
28. Munir ZA, Anselmi-Tamburini U, Ohyanagi M (2006) The effect of electric field and pressure on the synthesis and consolidation of materials: a review of the spark plasma sintering method. J Mater Sci 41:763–777. doi:10.1007/s10853-006-6555-2
29. Rasband WS, ImageJ, U.S. National Institutes of Health, Bethesda, Maryland, USA, http://imagej.nih.gov/ij/, 1997–2014